CHEMISTRY OF MATERIALS

Article

pubs.acs.org/cm

# Correlating the Lifetime and Fluorine Content of Iridium(III) Emitters in Green Light-Emitting Electrochemical Cells

Daniel Tordera,[†] Juan J. Serrano-Pérez,[†] Antonio Pertegás,[†] Enrique Ortí,[†] Henk J. Bolink,*[,†] Etienne Baranoff,[‡] Md. Khaja Nazeeruddin,[§] and Julien Frey*[,§]

[†]Instituto de Ciencia Molecular, Universidad de Valencia, C/Catedrático J. Beltrán 2, ES-46980 Paterna (Valencia), Spain

[‡]School of Chemistry, University of Birmingham, Edgbaston, B15 2TT, England

[§]Laboratory of Photonics and Interfaces, Institute of Chemical Sciences and Engineering, École Polytechnique Fédérale de Lausanne, CH-1015 Lausanne, Switzerland

Supporting Information

**ABSTRACT:** In light-emitting electrochemical cells, the lifetime of the device is intrinsically linked to the stability of the phosphorescent emitter. In this study, we present a series of ionic iridium(III) emitters based on cyclometalating phenylpyridine ligands whose fluorine substituents are varied in terms of position and number. Importantly, despite these structural modifications, the emitters exhibit virtually identical electrochemical and spectroscopic properties, which allows for proper comparison in functional devices. Quantum-chemical calculations support the properties measured in solution and suggest great similarities regarding the electronic structures of the emitters. In electroluminescent devices, the initial luminance, efficiency, and efficacy are also relatively unaffected throughout the series. However, a shorter device lifetime is obtained upon increasing the fluorine content of the emitter, which suggests drawbacks of such electron-withdrawing substituents for the design of ionic iridium(III) emitters.

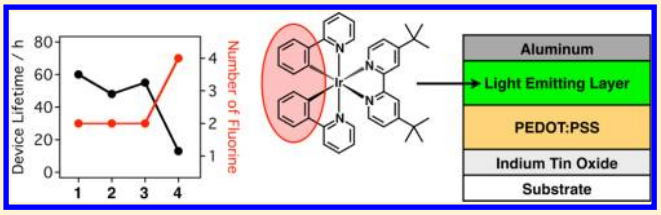


**KEYWORDS:** *electroluminescent devices, iridium emitters, stability*

## INTRODUCTION

Lighting accounts for about 20% of the worldwide energy consumption, which strongly motivates the development of energy-saving solutions such as organic light-emitting diodes (OLEDs).[1,2] Current OLED technologies are based on a multilayer architecture that combines low-weight active molecules with air-sensitive injection layers and metals.[3] The stack is most commonly obtained by sequential evaporation and requires rigorous encapsulation to prevent degradation.[4−6] Undoubtedly, the device architecture and the fabrication method must be simplified to reduce processing costs and allow for large-area applications.

In this context, light-emitting electrochemical cells (LECs) emerge as a promising alternative.[7] Their device architecture is dictated by the presence of mobile ions within the emitting layer. Upon the application of an external bias, the device experiences an ionic motion toward the electrodes that creates an in situ electrochemical doping. This dynamic doping renders the operation independent of the work function of the electrodes,[8] and suppresses the need for charge injection layers or metallic cathodes with poor ambient stability.[9] Consequently, LECs can be reduced to a single active layer and can be prepared under ambient conditions using solution processing, including conventional printing technologies.[10,11]

One particular class of LECs uses ionic transition-metal complexes (iTMCs) as emitters.[12−15] Cyclometalated iridium(III) iTMCs are ideal as they possess high phosphorescence quantum yields[16,17] with wide color-tunability.[18−23] Furthermore, they can be readily accessed through the use of neutral N^N ancillary ligands[24,25] that derive from bipyridines.[26,27]

With this design, the emissive state of the iTMC usually involves charge transfer from the iridium center and the cyclometalated ligands to the ancillary ligand, and therefore has both metal-to-ligand and ligand-to-ligand charge-transfer character (MLCT and LLCT, respectively). To obtain blue-to-green emission, one approach consists of using a non-chromophoric ancillary ligand with a high-lying lowest-unoccupied molecular orbital (LUMO).[28,29] Alternatively, the highest-occupied molecular orbital (HOMO) of the emitter can be stabilized by introducing strong electron-withdrawing group(s) at the cyclometalating ligands.[30−32]

Fluorine electron-withdrawing substituents are usually preferred because the resulting iridium(III) emitters tend to exhibit higher photoluminescence quantum yields (PLQY) than their nonfluorinated counterparts,[33] which is essential to obtain efficient LECs. However, the electron-withdrawing character of the fluorine atom strongly polarizes the C−F bonds, which may explain their fragility in functional devices.[34] Additionally, as the energy content of the generated excitons

**Received:** June 17, 2013
**Published:** August 2, 2013

   dx.doi.org/10.1021/cm402473j | *Chem. Mater.* 2013, 25, 3391−3397

**Chart 1. Chemical Structures of iTMCs 1−4**[a]

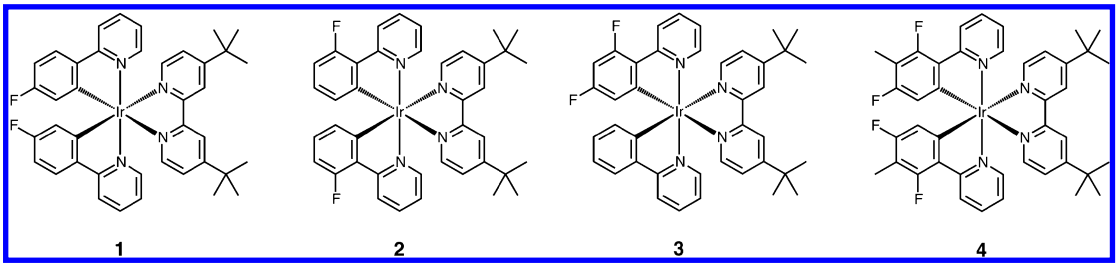


[a]Emitters were isolated and used in LECs as $PF_6^-$ salts.

increases (particularly for the blue), low-lying d−d states become thermally more accessible.[35−37] By nature, these metal-centered (MC) states have a dissociative character, and their population may lead to degradation through the formation of unsaturated iridium(III) species. The latter can react with surrounding molecules and generate phosphorescence quenchers in the active layer.[38,39]

Since blue and green LECs are much less stable than their orange counterparts, it is fundamental to understand the impact of the fluorine content of the emitter on the device lifetime. However, this task is not straightforward because of the working mechanism of LECs. In the absence of charge-transporting layers, charge-carrier migration in LECs depends on the iTMCs ability to transport both electrons and holes.[40] To compare relative stabilities throughout a series, it is therefore imperative to align the oxidation and reduction potentials while maintaining similar emissive properties.

Herein, we describe a series of green-emitting cyclometalated iridium(III) iTMCs (Chart 1) that differ in the number and the position of fluorine substituents, but whose photoelectrochemical properties are virtually identical in solution and thin solid films. Their performances are evaluated in a simple LEC architecture. Using a pulsed-current driving method, high luminances (ca. 1050 cd $m^{-2}$) are obtained regardless of the iTMC, with similar efficacies and efficiencies. However, we observe different kinetics in the performance degradation throughout the series. In an attempt to understand the factors influencing the stability, iTMCs **1−4** are investigated using quantum-chemical calculations, which provide information regarding the energy and nature of the lowest-lying triplet excited states and $^3$MC states. The present study highlights a potential "fluorine bottleneck" that is worthy of consideration in the design of more stable, efficient iridium iTMCs.

## EXPERIMENTAL DETAILS

**Electrochemical Properties.** Voltammetric measurements employed a PC controlled AutoLab PSTAT10 electrochemical workstation and were carried out under anaerobic conditions (argon filled glovebox, < 5 ppm $O_2$ and $H_2O$). Measurements were performed using 0.1 M tetrabutylammonium hexafluorophosphate in anhydrous acetonitrile and a set of carbon glassy, Pt plate, and Pt wire as working, counter, and quasi-reference electrode, respectively. Ferrocene was used as internal standard ($E^0$ = +0.64 V vs NHE).[41] A scan rate of 1000 mV $s^{-1}$ was applied.

**Photophysical Properties.** Electronic spectroscopic data were collected in nitrogen degassed solutions using a Hewlett-Packard 8453 spectrophotometer. The quantum yields were determined using fluorescein ($10^{-5}$ M in 0.1 M NaOH; air equilibrated; PLQY = 0.93) as standard.[42] Emission spectra were recorded with a Fluorolog Horiba Jobin Yvon Model FL-1065, and excited-state lifetimes were measured following 406 nm Nanoled excitation. The photoluminescence spectra and quantum yields of the thin films were measured with a Hamamatsu C9920-02 Absolute PLQY Measurement System ($\lambda_{exc}$ = 315 nm). The system is made of an excitation light source, consisting of a xenon lamp linked to a monochromator, an integration sphere, and a multichannel spectrometer.

**Computational Details.** Density functional theory (DFT)[43−45] calculations were carried out with the C.01 revision of the Gaussian 09 program package,[46] using Becke's three-parameter B3LYP exchange-correlation functional[47,48] together with the 6-31G** basis set for C, H, N, and F,[49] and the "double-ζ " quality LANL2DZ basis set for the Ir element.[50] The geometries of the singlet ground state ($S_0$), the lowest-energy triplet state ($T_1$), and the lowest-lying metal-centered ($^3$MC) state of the $[Ir(C^N)_2(dtb\text{-}bpy)]^+$ cations of complexes **1−4** were fully optimized by imposing $C_2$ symmetry constraints except for complex **3** which exhibits no symmetry. The geometries of the triplet states were calculated at the spin-unrestricted UB3LYP level. The nature of the obtained stationary points was confirmed as energy minima in all the cases by carrying out frequency calculations (and after analyzing the analytic second derivatives).

All the calculations were performed in the presence of the solvent (acetonitrile). Solvent effects were considered within the self-consistent reaction field (SCRF) theory using the SMD keyword that performs a polarized continuum model (PCM)[51,52] calculation using the solvation model of Truhlar et al.[53] The SMD solvation model is based on the polarized continuous quantum chemical charge density of the solute.

Time-dependent DFT (TD-DFT) calculations[54,55] of the lowest-lying triplet states were performed in the presence of the solvent at the minimum-energy geometry optimized for the ground state. Specifically, the lowest-lying 40 triplet excited states of complexes **2** and **4** were computed at the TD-DFT level and, in addition, the three lowest-lying triplet excited states were fully optimized at this level of theory to confirm the nature of the emitting state.

**Device Preparation.** The solvents were supplied by Aldrich. The thickness of films was determined with an Ambios XP-1 profilometer. Indium tin oxide ITO-coated glass plates (15 Ω $sq^{-1}$) were patterned by conventional photolithography (www.naranjosubstrates.com). The substrates were cleaned by successive 10 min sonication periods in water-soap, then water, and finally 2-propanol baths. After drying, the substrates were placed in a UV-ozone cleaner (Jelight 42-220) for 20 min. The electroluminescence devices were prepared as follows. First, a 90-nm layer of poly(3,4-ethylenedioxythiophene):poly(styrenesulfonate) (PEDOT:PSS) (CLEVIOS P VP AI 4083, aqueous dispersion, 1.3−1.7% solid content, Heraeus) was spin-coated on the ITO glass substrate to improve the reproducibility of the devices and to prevent the formation of pinholes. Then, 90-nm films (consisting of one of the emitters **1−4** and the 1-butyl-3-methylimidazolium hexafluorophosphate $[BMIM^+][PF_6^-]$ ionic liquid (>98.5%, Sigma-Aldrich) at a molar ratio of 4 to 1) were spin-coated from 20 mg $mL^{-1}$ acetonitrile solution at 1000 rpm for 20 s. The devices were transferred to an inert atmosphere glovebox (<0.1 ppm $O_2$ and $H_2O$, MBraun) and annealed at 100 °C for 1 h. Finally, using a shadow mask, the aluminum electrode (70 nm) was thermally evaporated under vacuum (<1 × $10^{-6}$ mbar) with an Edwards Auto500 evaporator integrated in the glovebox. The area of the device was 6.534 $mm^2$. The devices were not encapsulated and were characterized inside the glovebox at room temperature.


dx.doi.org/10.1021/cm402473j | Chem. Mater. 2013, 25, 3391−3397

Table 1. Electrochemical and Photophysical Properties of Emitters 1−4

| | $E_{OX}$[a]/V | $E_{RED}$[a]/V | $\lambda_{max}^{sol}$[b]/nm | $\tau$[c]/$\mu$s | $\Phi_{PL}^{sol}$ | $k_r$[d]/$10^5$ $s^{-1}$ | $k_{nr}$[d]/$10^5$ $s^{-1}$ | $\lambda_{max}^{glass}$[e]/nm | $\lambda_{max}^{film}$[f]/nm | $\Phi_{PL}^{film}$ | $\lambda_{max}^{dev}$[e]/nm | $\Phi_{PL}^{devg}$ |
|---|---|---|---|---|---|---|---|---|---|---|---|---|
| 1 | +1.02 | −1.84 | 552 | 1.06 | 0.69 | 6.48 | 2.91 | 460 | 505 | 0.82 | 538 | 0.48 |
| 2 | +1.00 | −1.83 | 555 | 0.55 | 0.52 | 7.64 | 10.5 | 463 | 519 | 0.89 | 540 | 0.57 |
| 3 | +1.00 | −1.83 | 555 | 0.99 | 0.59 | 5.99 | 4.16 | 464 | 514 | 0.84 | 544 | 0.59 |
| 4 | +1.03 | −1.83 | 554 | 0.78 | 0.62 | 9.23 | 3.59 | 456 | 503 | 0.93 | 534 | 0.66 |

[a]Measured in acetonitrile, potential vs $Fc^+/Fc$. [b]Nitrogen saturated $10^{-5}$ M solution in acetonitrile, excitation at 320 nm. [c]Excitation at 406 nm. [d]Assuming unitary intersystem crossing, $k_r = \Phi/\tau$ and $k_{nr} = (1-\Phi)/\tau$. [e]Nitrogen saturated $10^{-5}$ M solution in 2-methyltetrahydrofuran at 77 K, excitation at 320 nm. [f]5 wt % in PMMA thin film, excitation at 315 nm. [g]Thin film of complex with 1-butyl-3-methylimidazolium hexafluorophosphate (4:1 ratio).

**Device Characterization.** An Avantes luminance spectrometer was used to measure the EL spectrum. Device lifetime was measured by applying pulsed currents and monitoring the voltage and luminance by a True Color Sensor MAZeT (MTCSiCT Sensor) with a Botest OLT OLED Lifetime-Test System.

## RESULTS AND DISCUSSION

**Electrochemical and Photophysical Studies.** The structures of emitters **1**−**4** selected for this study are depicted in Chart 1. Each complex incorporates a different pair of 2-phenylpyridine (ppy) cyclometalating ligands along with a 4,4′-di-*tert*-butyl-2,2′-bipyridine ancillary ligand (dtb-bpy). Emitter **1** bears two fluorine atoms at the 4-position of each ppy ligand (4-Fppy) and was originally designed for its high PLQY.[56] Emitter **2**, an isomer of **1**, contains these fluorine atoms at the 2-position of each ppy ligand (2-Fppy). In contrast, emitter **3** is a tris-heteroleptic complex where both fluorine atoms are located at the 2- and 4-position of the same ligand.[57] Despite the structural modification, complex **3** exhibits photoelectrochemical properties that are similar to those of **1** and **2**. Finally, the ppy ligand of complex **4** contains a total of four fluorine atoms at both the 2- and 4-positions of each ppy ligand, along with a 3-methyl substituent (2,4-diF-3-Me-ppy). Because of the increased number of fluorine atoms, an electron-donating 3-methyl group is introduced to maintain the photoelectrochemical properties of emitters **1**−**3** and to avoid degradation issues linked to the acidity of the proton in this position.[58] The complexes were prepared using standard procedures (see the Supporting Information).[57]

The electrochemical properties of **1**−**4** were determined in acetonitrile using cyclic voltammetry and differential pulse voltammetry techniques. Data are presented in Table 1 vs the ferrocenium/ferrocene couple ($Fc^+/Fc$). All four complexes exhibit a quasi-reversible one-electron oxidation at potentials ranging from 1.00 to 1.03 V, and a quasi-reversible one-electron reduction around −1.83 V (Supporting Information, Figures S17 and S18), which results in electrochemical gaps, $\Delta E = E_{OX} - E_{RED}$, between 2.83 and 2.86 V. As expected, the four complexes also have similar optical characteristics. The UV−vis absorption spectra of complexes **1**−**4** in acetonitrile are displayed in Figure 1. All four complexes exhibit strong absorption bands below 320 nm that originate from spin-allowed $^1\pi-\pi^*$ ligand-centered (LC) transitions. Less structured bands in the 320−420 nm range are assigned to $\pi-\pi^*$ LLCT transitions and to MLCT transitions with singlet and triplet spin multiplicity.

The emission spectra of the complexes were recorded in acetonitrile at room temperature (RT, 298 K), and in 2-methyltetrahydrofuran glass at 77 K. Following excitation at 320 nm within the $\pi-\pi^*$ and MLCT absorption bands, broad and nonstructured emissions with maxima at 552, 555, 555, and 554 nm are observed at RT for **1**, **2**, **3**, and **4**, respectively. The

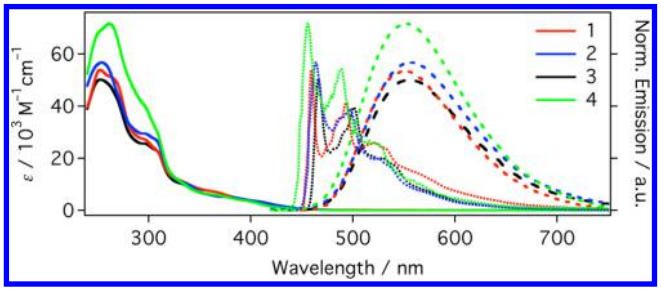


**Figure 1.** Absorption (solid) and normalized emission spectra of compounds **1**−**4** at RT in acetonitrile (dashed), and at 77 K in 2-methyltetrahydrofuran (dotted).

emission profiles are characteristic of complexes containing a combination of cyclometalated and neutral ancillary ligands. At 77 K, the spectra become highly structured and the emission maxima blue-shift to 460, 463, 464, and 456 nm. The observed rigidochromic effect suggests a strong MLCT character of the emissive state.[59] The excited-state lifetimes and PLQY of the compounds lie within the same order of magnitude, with emitter **2** being slightly less emissive than the others. This decrease in the PLQY could be due to a geometrical deformation in the excited state compared to complex **1**.[60] A similar shift is expected for complexes **3** and **4**; however, the PLQY can also improve with decreasing vibrational modes.[33,61]

The photoluminescence of the complexes was also studied in thin solid films. The complexes were either dispersed 5 wt % in a polymethylmethacrylate (PMMA) matrix or mixed in a 4 to 1 molar ratio with the 1-butyl-3-methylimidazolium hexafluorophosphate $[BMIM^+][PF_6^-]$ ionic liquid (IL) for the active layer of the device. In the PMMA films, we observe virtually identical, broad, nonstructured emission as shown in Figure 2a. The spectra are blue-shifted compared to those recorded in acetonitrile solutions with emission maxima at 505, 519, 514,

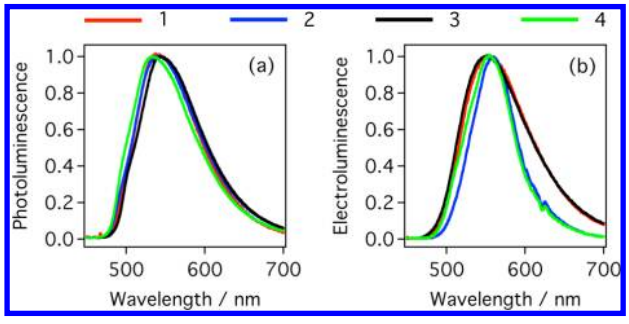


**Figure 2.** (a) Photoluminescence of PMMA thin films and (b) electroluminescence of LECs containing **1**−**4**. PL: 5 wt % emitter in PMMA; EL: ITO/PEDOT:PSS/iTMC:IL/Al at an applied bias of 100 A $m^{-2}$.


dx.doi.org/10.1021/cm402473j | Chem. Mater. 2013, 25, 3391−3397

and 503 nm for **1**, **2**, **3**, and **4**, respectively. The shoulder observed around 480 nm is a result of the rigidity of the PMMA film, which affects the optical transition and explains the increase in PLQY. The lower PLQY measured in the IL films ($\Phi_{PL}^{dev}$) are indicative of quenching phenomena due to higher iTMC concentrations.[62]

**Theoretical Calculations.** To gain a deeper insight into the electrochemical and photophysical properties of the emitters, density functional theory (DFT) calculations were carried out at the B3LYP/(6-31G* + LANL2DZ) level. Almost identical energies (±0.02 eV) are obtained for the HOMO ($E_{HOMO}$) and LUMO ($E_{LUMO}$) of complexes **1**−**4** (Table 2),

**Table 2. HOMO ($E_{HOMO}$) and LUMO ($E_{LUMO}$) Energies, HOMO−LUMO Energy Gap ($E_{H-L}$), Adiabatic Energy Differences $\Delta E(T_1-S_0)$ and $\Delta E(^3MC-T_1)$, and Emission Energy from $T_1$ ($E_{em}$) Computed in Acetonitrile Solution[a]**

| | 1 | 2 | 3 | 4 |
|---|---|---|---|---|
| $E_{HOMO}$ | −5.56 | −5.58 | −5.57 | −5.58 |
| $E_{LUMO}$ | −1.96 | −1.97 | −1.96 | −1.99 |
| $E_{H-L}$ | 3.60 | 3.61 | 3.61 | 3.59 |
| $\Delta E(T_1-S_0)$ | 2.63 | 2.62 | 2.62 | 2.63 |
| $\Delta E(^3MC-T_1)$ | 0.20 | 0.21 | 0.17 | 0.26 |
| $E_{em}$ | 2.36 | 2.35 | 2.35 | 2.36 |

[a]All energy values are reported in eV.

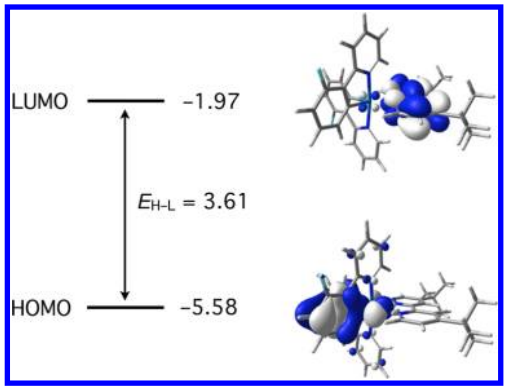


**Figure 3.** Energies (in eV) and electron density contours (0.03 e·bohr$^{-3}$) calculated for the HOMO and LUMO of complex **2**.

thus supporting the measured redox potentials. Figure 3 shows the energies and electronic density contours calculated for the HOMO and LUMO of complex **2** as a representative example. The HOMO is composed of a mixture of d orbitals of Ir(III) and phenyl $\pi$ orbitals of the cyclometalated ligands, whereas the LUMO is composed of $\pi$ orbitals of the ancillary ligand with a small contribution from the Ir(III) center.

To confirm the MLCT/LLCT nature of the emissive state, the lowest-energy triplet ($T_1$) of complexes **1**−**4** was calculated using the spin-unrestricted UB3LYP approach (and further confirmed by TD-DFT calculations, see the Supporting Information). After full-geometry relaxation, the $T_1$ triplet shows the unpaired-electron spin-density distribution displayed in Figure 4b for complex **2** (Ir: 0.51e; 2-Fppy: 0.47e; dtb-bpy: 1.02e) that matches the combined topologies of the HOMO and the LUMO. The difference in electron density between $T_1$ and the ground state $S_0$ depicted in Figure 4c clearly illustrates an electron transfer from the Ir-phenyl environment to the

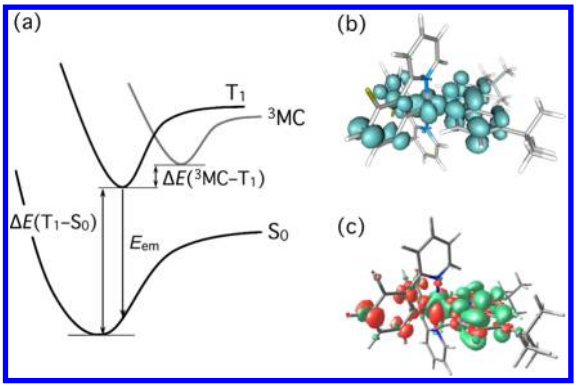


**Figure 4.** (a) Schematic illustration of the relative energies of the $S_0$, $T_1$, and $^3$MC states for emitters **1**−**4**. (b) Spin-density distribution (0.003 e·bohr$^{-3}$) calculated for the $T_1$ state of **2**. (c) Difference electron density (0.002 e·bohr$^{-3}$), computed by subtracting the electron densities of the $T_1$ and $S_0$ states for complex **2**. The charge goes from the red to the green areas. Differences in Mulliken atomic charges between $T_1$ and $S_0$ are +0.22, +0.49, and −0.71e for Ir, 2-Fppys, and dtb-bpy, respectively.

diimine ligand that takes place in passing from $S_0$ to the excited $T_1$ state.[12,63] Identical trends are obtained for complexes **1**, **3** and **4** (Supporting Information, Figure S19). The calculated adiabatic energy difference between the energy minima of the $S_0$ and $T_1$ states ($\Delta E(T_1-S_0)$) and the emission energy from the $T_1$ state ($E_{em}$)[64] are presented in Table 2 and remain consistent across the series.

The thermal accessibility of the $^3$MC excited state from the emitting $T_1$ state is known to strongly influence LECs performances, in particular the stability.[65,66] $^3$MC states result from excitation of an electron from the occupied $t_{2g}$ ($d\pi$) orbitals to the unoccupied $e_g$ orbitals of the metal (Figure 5a).

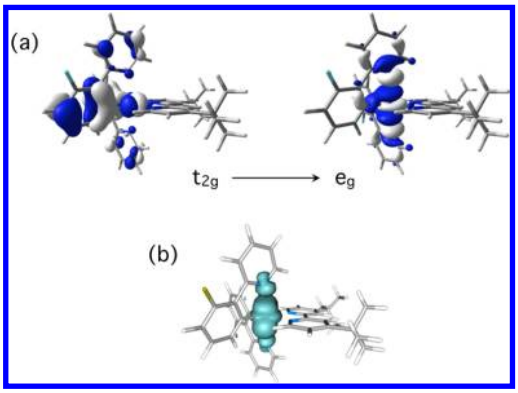


**Figure 5.** (a) Electron density contours (0.03 e·bohr$^{-3}$) calculated for the two SOMOs (singly occupied molecular orbitals) of the lowest-lying $^3$MC excited state of complex **2**. (b) Spin-density distribution (0.003 e·bohr$^{-3}$) computed for the $^3$MC of **2**.

The $e_g$ orbital has a $d\sigma^*$-antibonding character, and its population may lead to the formation of unstaturated, reactive species. To analyze the influence of the $^3$MC states on the electronic structure of complexes **1**−**4**, these states were investigated at the UB3LYP level starting from distorted geometries, in which the $N_{ppy}$ atoms are moved away from the Ir center.

After full-geometry relaxation, the Ir−$N_{ppy}$ bond distances of complex **2** lengthen from 2.080 Å in $S_0$ to 2.590 Å in the $^3$MC state. Similar bond elongations are reproduced for emitters **1**, **3**,


dx.doi.org/10.1021/cm402473j | Chem. Mater. 2013, 25, 3391−3397

and **4** (Supporting Information, Table S2). The spin-density calculated at the optimized geometry (Figure 5b) shows that most of the unpaired electrons (1.72e for **2**) are located on the iridium core, which further confirms the $^3$MC nature of the state. Most importantly, the adiabatic energy differences, $\Delta E(^3\text{MC}-\text{T}_1)$, are computed at similar values throughout the series, 0.20 (complex **1**), 0.21 (**2**), 0.17 (**3**), and 0.26 eV (**4**). Therefore, thermal population of the $^3$MC state should similarly influence the degradation of these emitters in LECs.

**Light-Emitting Devices.** To investigate the electroluminescent properties of emitters **1**−**4**, two-layer LECs were prepared by spin coating a 90 nm layer of PEDOT:PSS on a patterned indium tin oxide (ITO)-coated glass substrate, followed by a 90 nm emitting layer consisting of one of the emitters **1**−**4** and the $[\text{BMIM}^+][\text{PF}_6^-]$ IL at a molar ratio of 4 to 1. Finally, a 70 nm aluminum layer was thermally evaporated as cathode. Details concerning the preparation and characterization of the devices can be found in the Experimental Section.

The electroluminescent (EL) spectra show broad and unstructured emissions similar to the PL spectra measured in solution and in thin solid films, with emission maxima ($\lambda_{max}^{EL}$) at 554, 558, 552, and 555 nm (see Figure 2b). This indicates that, in the device configuration, the excited-state energies are comparable throughout the series (2.30 ± 0.02 eV). However, the shape of the EL spectra is affected by the structure of the ppy ligand. Emitters **1** ($x$ = 0.38, $y$ = 0.57) and **3** ($x$ = 0.39, $y$ = 0.56) exhibit broader emission than **2** ($x$ = 0.42, $y$ = 0.55) and **4** ($x$ = 0.39, $y$ = 0.55), which translates into different CIE coordinates. This difference is not fully understood, and it is tentatively assigned to differences in the film morphologies. Previous studies have demonstrated that amorphous spin-coated films consist of nm-sized crystalline domains.[67]

The initial EL performances of the device are not drastically affected by the nature of the emitter, as shown in Figures 6a−c and summarized in Table 3. All LECs exhibit a short turn-on time (<5 s) and reach their maximum efficiency after a few minutes, with comparable luminance (ca. 1050 cd m$^{-2}$), efficacy (9.6 to 10.4 cd A$^{-1}$), and power efficiency (5.2 to 5.4 lm W$^{-1}$). Under these comparable conditions, we observe similar lifetimes around 55 h for complexes **1**−**3**, with a linear

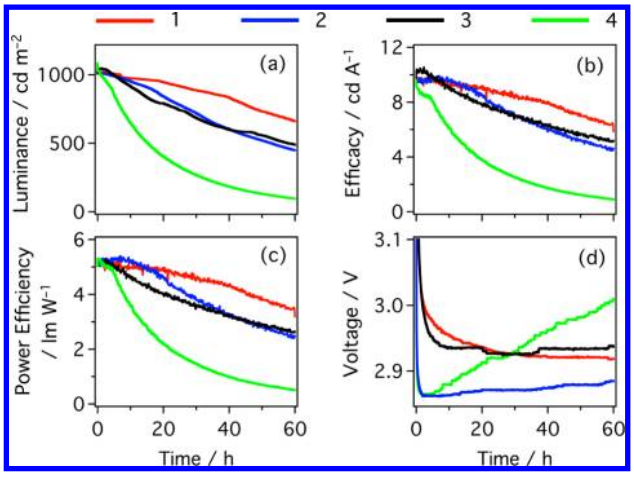


**Figure 6.** (a) Luminance, (b) efficacy, (c) power efficiency, and (d) voltage for ITO/PEDOT:PSS/iTMC:IL(4:1)/Al LECs incorporating emitters **1**−**4**. LECs were driven at a pulsed current with an average current density of 100 A m$^{-2}$, using a block wave at a frequency of 1000 Hz and a duty cycle of 50%.

**Table 3. Performance of LEC Devices Biased with a Block-Wave Pulsed Current at a Frequency of 1000 Hz, an Average Current of 100 A m$^{-2}$ with a Duty Cycle of 50%**

| | 1 | 2 | 3[a] | 4 |
|---|---|---|---|---|
| $n$(F)[b] | 2 | 2 | 2 | 4 |
| $\lambda_{max}^{EL}$/nm | 554 | 558 | 552 | 555 |
| Lum$_{max}$/cd m$^{-2}$ | 1028 | 1066 | 1046 | 1095 |
| $t_{1/2}$/h[c] | 59.8 | 48.3 | 55.0 | 13.2 |
| efficacy/cd A$^{-1}$ | 9.8 | 9.8 | 10.4 | 9.6 |
| power efficiency/lm W$^{-1}$ | 5.2 | 5.4 | 5.3 | 5.3 |
| EQE/%[d] | 2.85 | 2.92 | 2.99 | 2.90 |

[a]From ref 57. [b]Number of fluorine substituents. [c]Time to half of the luminance. [d]External quantum efficiency.

performance decrease. In contrast, LECs based on emitter **4**, the one incorporating four fluorine substituents, shows a 4-fold decrease in the lifetime (ca. 13 h), with exponential performance decay.

Under current-based driving conditions, the applied voltage rapidly decreases with the accumulation of ions at the electrodes (Figure 6d). This ionic motion creates doped regions within the active layer and lowers the electron and hole injection barriers. Eventually, the voltage reaches a steady state that maintains a balanced ionic transport within the active layer. While LECs incorporating emitters **1**−**3** follow this ideal behavior,[68] devices employing emitter **4** require a steady increase of voltage after only 2.5 h of operation.

Since emitters **1**−**4** exhibit comparable electrochemical and spectroscopic properties with similar electronic structures, this observation highlights the propensity of emitter **4** to degrade faster than the others, and demonstrates for the first time that higher fluorine content may be detrimental to the stability of the emitter in functional devices. Importantly, these results are in line with previously published results, where "parent" orange $[\text{Ir(ppy)(dtb-bby)}]^+$ and blueish-green $[\text{Ir(di-Fppy)(dtb-bby)}]^+$ emitters exhibited lifetimes of 370 and 3.3 h, respectively.[57]

## CONCLUSION

Throughout a series of $[\text{Ir(ppy)}_2\text{(dtb-bby)}]^+$ derivatives with similar electrochemical, spectroscopic, and electroluminescent properties, we show that LECs based on an emitter with four fluorine substituents (**4**) deteriorates remarkably fast relative to several emitters with two fluorine substituents (**1**−**3**). These results may indicate a correlation between fluorine content and stability of the emitters in functional devices. Therefore, although this electron-withdrawing group is convenient to tune the emissive properties of iridium(III) iTMCs, alternatives may be required to blue-shift the emission without sacrificing device stability.

## ASSOCIATED CONTENT

### Supporting Information

Synthetic procedures and characterizing data for experimentally studied compounds; supplemental figures discussed in the text. This material is available free of charge via the Internet at http://pubs.acs.org.

## AUTHOR INFORMATION

### Corresponding Author

*E-mail: henk.bolink@uv.es (H.J.B.), julien.frey@gmail.com (J.F.).

### Notes

The authors declare no competing financial interest.

## ■ ACKNOWLEDGMENTS

This work has been supported by the European Union (CELLO, Grant STRP 248043; https://www.cello-project.eu/), the Spanish Ministry of Economy and Competitiveness (MINECO) (MAT2011-24594, CSD2007-00010, and CTQ2012-31914), the Generalitat Valenciana (Prometeo/2012/053), and the European FEDER funds (CTQ2012-31914). D.T. and A.P. acknowledge MECD (Spanish Ministry of Education, Culture, and Sport) and MINECO for FPU and FPI grants, respectively.

## ■ REFERENCES

(1) Baldo, M. A.; Thompson, M. E.; Forrest, S. R. *Nature* **2000**, *403*, 750−753.
(2) Baldo, M. A.; Lamansky, S.; Burrows, P. E.; Thompson, M. E.; Forrest, S. R. *Appl. Phys. Lett.* **1999**, *75*, 4−6.
(3) Walzer, K.; Maennig, B.; Pfeiffer, M.; Leo, K. *Chem. Rev.* **2007**, *107*, 1233−1271.
(4) He, G.; Pfeiffer, M.; Leo, K.; Hofmann, M.; Birnstock, J.; Pudzich, R.; Salbeck, J. *Appl. Phys. Lett.* **2004**, *85*, 3911−3913.
(5) Pfeiffer, M.; Forrest, S. R.; Leo, K.; Thompson, M. E. *Adv. Mater.* **2002**, *14*, 1633−1636.
(6) Huang, J.; Pfeiffer, M.; Werner, A.; Blochwitz, J.; Leo, K.; Liu, S. *Appl. Phys. Lett.* **2002**, *80*, 139−141.
(7) Sandström, A.; Dam, H. F.; Krebs, F. C.; Edman, L. *Nat. Commun.* **2012**, *3*, 1002.
(8) van Reenen, S.; Matyba, P.; Dzwilewski, A.; Janssen, R. A. J.; Edman, L.; Kemerink, M. *J. Am. Chem. Soc.* **2010**, *132*, 13776−13781.
(9) Pei, Q.; Yu, G.; Zhang, C.; Yang, Y.; Heeger, A. J. *Science* **1995**, *269*, 1086−1088.
(10) Matyba, P.; Yamaguchi, H.; Chhowalla, M.; Robinson, N. D.; Edman, L. *ACS Nano* **2011**, *5*, 574−580.
(11) Mauthner, G.; Landfester, K.; Kock, A.; Bruckl, H.; Kast, M.; Stepper, C.; List, E. J. W. *Org. Electron.* **2008**, *9*, 164−170.
(12) Costa, R. D.; Ortí, E.; Bolink, H. J.; Monti, F.; Accorsi, G.; Armaroli, N. *Angew. Chem., Int. Ed.* **2012**, *51*, 8178−8211.
(13) Gao, F. G.; Bard, A. J. *J. Am. Chem. Soc.* **2000**, *122*, 7426−7427.
(14) Handy, E. S.; Pal, A. J.; Rubner, M. F. *J. Am. Chem. Soc.* **1999**, *121*, 3525−3528.
(15) Lyons, C. H.; Abbas, E. D.; Lee, J. K.; Rubner, M. F. *J. Am. Chem. Soc.* **1998**, *120*, 12100−12107.
(16) Matsushita, T.; Asada, T.; Koseki, S. *J. Phys. Chem. C* **2007**, *111*, 6897−6903.
(17) King, K. A.; Spellane, P. J.; Watts, R. J. *J. Am. Chem. Soc.* **1985**, *107*, 1431−1432.
(18) He, L.; Qiao, J.; Duan, L.; Dong, G.; Zhang, D.; Wang, L.; Qiu, Y. *Adv. Funct. Mater.* **2009**, *19*, 2950−2960.
(19) Costa, R. D.; Céspedes-Guirao, F. J.; Ortí, E.; Bolink, H. J.; Gierschner, J.; Fernández-Lázaro, F.; Sastre-Santos, A. *Chem. Commun.* **2009**, 3886−3888.
(20) Stagni, S.; Colella, S.; Palazzi, A.; Valenti, G.; Zacchini, S.; Paolucci, F.; Marcaccio, M.; Albuquerque, R. Q.; De Cola, L. *Inorg. Chem.* **2008**, *47*, 10509−10521.
(21) Di Censo, D.; Fantacci, S.; De Angelis, F.; Klein, C.; Evans, N.; Kalyanasundaram, K.; Bolink, H. J.; Grätzel, M.; Nazeeruddin, M. K. *Inorg. Chem.* **2008**, *47*, 980−989.
(22) Avilov, I.; Minoofar, P.; Cornil, J.; De Cola, L. *J. Am. Chem. Soc.* **2007**, *129*, 8247−8258.
(23) Slinker, J. D.; Gorodetsky, A. A.; Lowry, M. S.; Wang, J.; Parker, S.; Rohl, R.; Bernhard, S.; Malliaras, G. G. *J. Am. Chem. Soc.* **2004**, *126*, 2763−2767.
(24) Mydlak, M.; Bizzarri, C.; Hartmann, D.; Sarfert, W.; Schmid, G.; De Cola, L. *Adv. Funct. Mater.* **2010**, *20*, 1812−1820.
(25) He, L.; Duan, L.; Qiao, J.; Wang, R.; Wei, P.; Wang, L.; Qiu, Y. *Adv. Funct. Mater.* **2008**, *18*, 2123−2131.
(26) Parker, S. T.; Slinker, J. D.; Lowry, M. S.; Cox, M. P.; Bernhard, S.; Malliaras, G. G. *Chem. Mater.* **2005**, *17*, 3187−3190.
(27) Tamayo, A. B.; Garon, S.; Sajoto, T.; Djurovich, P. I.; Tsyba, I. M.; Bau, R.; Thompson, M. E. *Inorg. Chem.* **2005**, *44*, 8723−8732.
(28) Lowry, M. S.; Goldsmith, J. I.; Slinker, J. D.; Rohl, R.; Pascal, R. A., Jr.; Malliaras, G. G.; Bernhard, S. *Chem. Mater.* **2005**, *17*, 5712−5719.
(29) Slinker, J. D.; Koh, C. Y.; Malliaras, G. G.; Lowry, M. S.; Bernhard, S. *Appl. Phys. Lett.* **2005**, *86*, 173506.
(30) Bolink, H. J.; Coronado, E.; Costa, R. D.; Lardiés, N.; Ortí, E. *Inorg. Chem.* **2008**, *47*, 9149−9151.
(31) De Angelis, F.; Fantacci, S.; Evans, N.; Klein, C.; Zakeeruddin, S. M.; Moser, J.-E.; Kalyanasundaram, K.; Bolink, H. J.; Grätzel, M.; Nazeeruddin, M. K. *Inorg. Chem.* **2007**, *46*, 5989−6001.
(32) Liu, S.-H.; Fang, F.-C.; Hwu, T.-Y.; Hsieh, H.-H.; Chen, H.-F.; Lee, G.-H.; Peng, S.-M.; Wong, K.-T.; Wu, C.-C. *Adv. Funct. Mater.* **2007**, *17*, 1019−1027.
(33) Li, J.; Djurovich, P. I.; Alleyne, B. D.; Yousufuddin, M.; Ho, N. N.; Thomas, J. C.; Peters, J. C.; Bau, R.; Thompsom, M. E. *Inorg. Chem.* **2005**, *44*, 1713−1727.
(34) Sivasubramaniam, V.; Brodkorb, F.; Hanning, S.; Loebl, H. P.; van Elsbergen, V.; Boerner, H.; Scherf, U.; Kreyenschmidt, M. *J. Fluorine Chem.* **2009**, *130*, 640−649.
(35) Costa, R. D.; Ortí, E.; Bolink, H. J.; Graber, S.; Housecroft, C. E.; Constable, E. C. *Adv. Funct. Mater.* **2010**, *20*, 1511−1520.
(36) Bolink, H. J.; Coronado, E.; Costa, R. D.; Ortí, E.; Sessolo, M.; Graber, S.; Doyle, K.; Neuburger, M.; Housecroft, C. E.; Constable, E. C. *Adv. Mater.* **2008**, *20*, 3910−3913.
(37) Thompson, D. W.; Wishart, J. F.; Brunschwig, B. S.; Sutin, N. *J. Phys. Chem. A* **2001**, *105*, 8117−8122.
(38) de Moraes, I. R.; Scholz, S.; Lüssem, B.; Leo, K. *Org. Electron.* **2011**, *12*, 341−347.
(39) Kalyuzhny, G.; Buda, M.; McNeill, J.; Barbara, P.; Bard, A. J. *J. Am. Chem. Soc.* **2003**, *125*, 6272−6283.
(40) Lenes, M.; Garcia-Belmonte, G.; Tordera, D.; Pertegás, A.; Bisquert, J.; Bolink, H. J. *Adv. Funct. Mater.* **2011**, *21*, 1581−1586.
(41) Connelly, N. G.; Geiger, W. E. *Chem. Rev.* **1997**, *96*, 877−910.
(42) Shen, J.; Snook, R. D. *Chem. Phys. Lett.* **1989**, *155*, 583−586.
(43) Dreuw, A.; Head-Gordon, M. *Chem. Rev.* **2005**, *105*, 4009−4037.
(44) Mercero, J. M.; Matxain, J. M.; Lopez, X.; York, D. M.; Largo, A.; Eriksson, L. A.; Ugalde, J. M. *Int. J. Mass Spectrom.* **2005**, *240*, 37−99.
(45) Mattsson, A. E. *Science* **2002**, *298*, 759−760.
(46) Frisch, M. J. T.; Schlegel, H. B.; Scuseria, G. E.; Robb, M. A.; Cheeseman, J. R.; Scalmani, G.; Barone, V.; Mennucci, B.; Petersson, G. A.; Nakatsuji, H.; Caricato, M.; Li, X.; Hratchian, H. P.; Izmaylov, A. F.; Bloino, J.; Zheng, G.; Sonnenberg, J. L.; Hada, M.; Ehara, M.; Toyota, K.; Fukuda, R.; Hasegawa, J.; Ishida, M.; Nakajima, T.; Honda, Y.; Kitao, O.; Nakai, H.; Vreven, T.; Montgomery, J. A., Jr; Peralta, J. E.; Ogliaro, F.; Bearpark, M.; Heyd, J. J.; Brothers, E.; Kudin, K. N.; Staroverov, V. N.; Kobayashi, R.; Normand, J.; Raghavachari, K.; Rendell, A.; Burant, J. C.; Iyengar, S. S.; Tomasi, J.; Cossi, M.; Rega, N.; Millam, N. J.; Klene, M.; Knox, J. E.; Cross, J. B.; Bakken, V.; Adamo, C.; Jaramillo, J.; Gomperts, R.; Stratmann, R. E.; Yazyev, O.; Austin, A. J.; Cammi, R.; Pomelli, C.; Ochterski, J. W.; Martin, R. L.; Morokuma, K.; Zakrezewski, V. G.; Voth, G. A.; Salvador, P.; Dannenberg, J. J.; Dapprich, S.; Daniels, A. D.; Farkas, O.; Foresman, J. B.; Ortiz, J. V.; Cioslowski, J.; Fox, D. J. *Gaussian 09*; Gaussian, Inc.: Wallingford, CT, 2009.
(47) Becke, A. D. *J. Chem. Phys.* **1993**, *98*, 5648−5652.
(48) Lee, C.; Yang, W.; Parr, R. G. *Phys. Rev. B* **1988**, *37*, 785−789.
(49) Francl, M. M.; Pietro, W. J.; Hehre, W. J.; Binkley, J. S.; Gordon, M. S.; DeFrees, D. J.; Pople, J. A. *J. Chem. Phys.* **1982**, *77*, 3654−3665.
(50) Hay, P. J.; Wadt, W. R. *J. Chem. Phys.* **1985**, *82*, 299−310.
(51) Tomasi, J.; Mennucci, B.; Cammi, R. *Chem. Rev.* **2005**, *105*, 2999−3094.

(52) Tomasi, J.; Persico, M. *Chem. Rev.* **1994**, *94*, 2027−2094.
(53) Marenich, A. V.; Cramer, C. J.; Truhlar, D. G. *J. Phys. Chem. B* **2009**, *113*, 6378−6396.
(54) Adamo, C.; Jacquemin, D. *Chem. Soc. Rev.* **2013**, *42*, 845−856.
(55) Marques, M. A. L.; Gross, E. K. U. *Annu. Rev. Phys. Chem.* **2004**, *55*, 427−455.
(56) Tordera, D.; Frey, J.; Vonlanthen, D.; Constable, E. C.; Pertegás, A.; Ortí, E.; Bolink, H. J.; Baranoff, E.; Nazeeruddin, M. K. *Adv. Energy Mater.* **2013**, ASAP. DOI: 10.1002/aenm.201300284.
(57) Tordera, D.; Delgado, M.; Ortí, E.; Bolink, H. J.; Frey, J.; Nazeeruddin, M. K.; Baranoff, E. *Chem. Mater.* **2012**, *24*, 1896−1903.
(58) Schlosser, M.; Heiss, C. *Eur. J. Org. Chem.* **2003**, 4618−4624.
(59) Tamayo, A. B.; Alleyne, B. D.; Djurovich, P. I.; Lamansky, S.; Tsyba, I.; Ho, N. N.; Bau, R.; Thompson, M. E. *J. Am. Chem. Soc.* **2003**, *125*, 7377−7387.
(60) Baranoff, E.; Curchod, B. F. E.; Monti, F.; Steimer, F.; Accorsi, G.; Tavernelli, I.; Rothlisberger, U.; Scopelliti, R.; Grätzel, M.; Nazeeruddin, M. K. *Inorg. Chem.* **2011**, *51*, 799−811.
(61) Sajoto, T.; Djurovich, P. I.; Tamayo, A. B.; Oxgaard, J.; Goddard, W. A., III; Thompson, M. E. *J. Am. Chem. Soc.* **2009**, *131*, 9813−9822.
(62) Rothe, C.; Chiang, C.-J.; Jankus, V.; Abdullah, K.; Zeng, X.; Jitchati, R.; Batsanov, A. S.; Bryce, M. R.; Monkman, A. P. *Adv. Funct. Mater.* **2009**, *19*, 2038−2044.
(63) Costa, R. D.; Ortí, E.; Bolink, H. J. *Pure Appl. Chem.* **2011**, *83*, 2115−2128.
(64) $E_{em}$ was calculated as the vertical energy difference between $T_1$ and $S_0$ by performing a single-point calculation of $S_0$ at the optimized minimum-energy geometry of $T_1$.
(65) Costa, R. D.; Monti, F.; Accorsi, G.; Barbieri, A.; Bolink, H. J.; Ortí, E.; Armaroli, N. *Inorg. Chem.* **2011**, *50*, 7229−7238.
(66) Costa, R. D.; Ortí, E.; Bolink, H. J.; Graber, S.; Schaffner, S.; Neuburger, M.; Housecroft, C. E.; Constable, E. C. *Adv. Funct. Mater.* **2009**, *19*, 3456−3463.
(67) Blasini, D. R.; Rivnay, J.; Smilgies, D.-M.; Slinker, J. D.; Flores-Torres, S.; Abruña, H. D.; Malliaras, G. G. *J. Mater. Chem.* **2007**, *17*, 1458−1461.
(68) Tordera, D.; Meier, S.; Lenes, M.; Slinker, J. D.; Costa, R. D.; Ortí, E.; Sarfert, W.; Bolink, H. J. *Adv. Mater.* **2012**, *24*, 890−897.